THESIS FOR THE DEGREE OF LICENTIATE OF ENGINEERING

Supervisory control for emission compliance of heavy-duty vehicles

MOHAMMED RAZAUL KARIM

CHALMERS

UNIVERSITY OF TECHNOLOGY

Department of Electrical Engineering
Chalmers University of Technology
Gothenburg, Sweden, 2020

Supervisory control for emission compliance of heavy-duty vehicles

MOHAMMED RAZAUL KARIM

This thesis has been prepared using LaTeX.

To my father, died in a road traffic accident with a heavy-duty truck while I was doing this research.

Abstract

Heavy freight trucks globally contribute to a significant proportion of transport-related air pollution. The dominant air pollutants from heavy freight trucks with diesel engine and exhaust aftertreatment system (EATS) are CO_2, hydrocarbons (HC), CO, particulate matter (PM), NO_x (NO and NO_2), and NH_3. The greenhouse gas emission legislation limits the amount of CO_2 emission, and Euro VI emission legislation limits the other dominant air pollutants. Emission legislation is gradually becoming more and more stringent to reach the long term goal of near-zero-emission. Several parties are working together to reduce the emissions, keeping both the short and long term goal in mind. Any step which results in ICE downsizing contributes to the reduction of all dominant emissions. But, with size and type of the ICE decided, there is a trade-off between NO_x emission and other emissions: reduced NO_x emission means reduced fuel efficiency (i.e. increased CO_2, PM, and HC emissions).

It is a challenge to fulfil the current emission legislation—especially real-driving NO_x emission legislation—with existing control functionalities in the engine management system (EMS). However, better control of NO_x emission is possible by exploiting predictive driving information and considering the coupling between the engine system and EATS. This work pursues this idea and concludes that fulfilling real-driving NO_x emission legislation is possible, considering the coupling between the engine system and EATS while using predictive information. The work provides a mathematical formulation of the concept and then develops, evaluates, and implements an engine-EATS supervisor which optimizes total fuel consumption and fulfils both the world harmonized transient cycle (WHTC) based and real-driving NO_x emission legislation. The developed supervisor is a distributed economic nonlinear model predictive controller (E-NMPC). This work develops and analyzes two different versions of the distributed E-NMPC based supervisory control algorithm. The more efficient one of the two is again compared for three variants. Considering the computation time of the three algorithms and processing speed of the existing EMS, one algorithm is selected for implementation.

The supervisor performs much better compared to a baseline controller (optimized offline). Simulation results show that the supervisory controller has 1.7% less total fuel consumption and 88.4% less NH_3 slip, compared to the baseline controller, to achieve the same real-driving NO_x emission.

Keywords: Diesel engines, exhaust aftertreatment system, Euro VI emission legislation, supervisory control, Pontryagin's minimum principle, E-NMPC.

ii

List of Publications

This thesis is based on the following publications:

[A] **Mohammed R. Karim**, Nikolce Murgovski, Esteban R. Gelso, and Bo Egardt, "Supervisory Framework and Model-based Control of Engine and Exhaust Aftertreatment System". Published in European Control Conference (ECC) 2018.

[B] **Mohammed R. Karim**, Bo Egardt, Nikolce Murgovski, and Esteban R. Gelso, "Supervisory Control for Real-Driving Emission Compliance of Heavy-Duty Vehicles". Published in 5$^{\text{th}}$ IFAC Conference on Engine and Powertrain Control, Simulation and Modeling E-COSM 2018.

[C] **Mohammed R. Karim**, Bo Egardt, Esteban R. Gelso, and Nikolce Murgovski, "Supervisory Control for NO$_\text{x}$ Emission Compliance of Heavy-Duty Vehicles". Submitted to IEEE Transactions on Vehicular Technology.

Other publication by the author, not included in this thesis, is:

[D] G. Vagnoni, S. Petri, F. Aubeck, J. Lindberg, E.R. Gelso, N. Mugovski, **Mohammed R. Karim**, J. Schaub, and A. Pantaleo, "Predictive Engine and Aftertreatment Control Concepts for a Heavy-Duty Long-Haul Truck". 27th Aachen Colloquium Automobile and Engine Technology, 2018.

iv

Acknowledgments

I am grateful to my both supervisors professor Bo Egardt and associate professor Nikolce Murgovski for their teaching, guidance and patience, and Esteban R. Gelso from AB Volvo for all of his support during this research work. I especially thank professor Bo Egardt for his mental support during my difficult time after my father's fatal accident with a heavy-duty truck.

Acronyms

ASC:	Ammonia slip catalyst
BMS:	Battery management system
CAC:	Charge-air cooler
CPU:	Central processing unit
DEF:	Diesel exhaust fluid
DLL:	Dynamic link library
DOC:	Diesel oxidation catalyst, Direct optimal control
DP:	Dynamic programming
DPF:	Diesel particulate filter
EATS:	Exhaust aftertreatment system
EGR:	Exhaust gas recirculation
EECU:	Engine electronic control unit
EMS:	Engine management system
E-NMPC:	Economic nonlinear model predictive control
HC:	Hydrocarbons

ICE:	Internal combustion engine
ITV:	Intake throttle valve
OCE:	Off-cycle emission
OCP:	Optimal control problem
PEMS:	Portable emissions measurement system
PM:	Particulate matter
PMP:	Pontryagin's minimum principle
SC-FAM:	Supervisory controller with function approximation of maps
SCR:	Selective catalytic reduction
SC-SLI:	Supervisory controller with scattered linear interpolation
SIL:	Software-in-the-loop
SLI:	Scattered linear interpolation
SoC:	State-of-charge
SQP:	Sequential quadratic programming
TC:	Turbo compound
WBW:	Work-based-window
WHSC:	World harmonized static cycle
WHTC:	World harmonized transient cycle

Contents

Part I

Overview

CHAPTER 1

Introduction

Road freight transport globally contributes to an increasing amount of CO_2 emissions. In 2015, the road freight accounted for 57% of total freight-related CO_2 emissions. The freight transport shared 36% of total transport-related CO_2 emissions in the same year, and current prediction is that the share would increase to 48% by 2050 [1].

Efforts are ongoing for electrification and hybridization of the road freight, which can significantly reduce the CO_2 emissions. But, in the short or medium term, the use of long-haul heavy freight trucks with near-zero-emission propulsion system would not be widespread [1]. In other words, the internal combustion engine (ICE) would continue to be used extensively in the heavy-duty propulsion system in the next decade. During operation, the ICE emitted gasses consists of Nitrogen, Oxygen, water vapour, and many air pollutants which are harmful to both environment and health. Besides CO_2, the dominant air pollutants from the ICE are hydrocarbons (HC), CO, particulate matter (PM), NO, and NO_2.

Vehicle emission standard is gradually becoming more and more stringent to fulfil the long term goal of near-zero-emission of harmful species. Automotive industries are introducing new technologies to cope with the changing emission legislation. Euro VI emission legislation for heavy-duty diesel vehicles limits the emission of

HC, CO, PM, NO_x (NO and NO_2), and NH_3. An initial reduction of the pollutants from the diesel vehicles is made through the improvement of the ICE design and control strategy —some examples are provided in [2]–[6]. Introduction of exhaust aftertreatment system (EATS) further decreases HC, CO, PM and NO_x from the exhaust gases but introduces secondary emissions, such as NO_2, N_2O, and NH_3 [7]. The legislation targets both primary and secondary emissions from ICE and EATS, respectively. Currently, vehicle industries are mainly facing problem to fulfil the constraint on NO_x compared to the limits on other pollutants in the Euro VI emission legislation.

In addition to the Euro VI emission legislation, greenhouse gas emission legislation for heavy-duty vehicles limits the amount of CO_2 emission. Emission of CO_2 is directly linked to fuel consumption by the ICE, i.e. reduction of the fuel consumption means a decrease in CO_2 emission. One way to decrease both the fuel consumption and NO_x emission is downsizing of the ICE. Turbocharging the ICE, improving the fuel efficiency of powertrains, redesigning vehicle body for reduced aerodynamic drag, decreasing tires' rolling resistance, and hybridizing the vehicles contributes to downsizing of the ICE [8]–[11]. In addition, governments and companies are investing in road infrastructure improvement, including intelligent transportation system networks establishment and roads' rolling resistance reduction [12]–[14], which reduces energy demand. More efficient operation of the vehicle also reduces energy demand; e.g., optimizing vehicle speeds and gear-shifting strategy, efficient route planning, vehicle platooning, more autonomous driving functionalities, and driver training [15]–[19]. Reduced energy demand results in a decrease in both CO_2 and NO_x emission. For a fixed ICE, in general, there is a trade-off between fuel consumption (i.e. CO_2 emission) and NO_x emission.

Engine systems become more complex as a result of more stringent legislation, and the operation of the engine, in turn, gets more complicated. With size and type of the ICE decided, optimizing fuel consumption and fulfilling the constraints on pollutants are the main goals set for an engine management system (EMS) that controls multiple engine actuators.

The EMS is used for control, diagnosis, monitoring, and safety of the engine. Diesel engine EMS' control functionalities include optimizing fuel consumption, reducing engine-out emissions, fulfilling requested torque from the driver, and keeping lower engine sound level [20]. It receives feedback signals using analogue and digital sensors, communicates with other units using internal communication network (e.g., CAN and FlexRay), and calculates output signals (e.g., control signals for the actu-

ators) using a central processing unit (CPU). It also converts low power CPU output to high power output for the actuators using output drivers. The intelligent actuators have their control module and need only setpoint trajectories from the CPU.

The existing control functionalities of EMS have a few major limitations. Firstly, the control algorithms are mostly based on experience and rely heavily on rule and map based solutions with many manually tunable parameters. Consequently, dependencies between functionality become hard to understand, and the effort to further evolve the system becomes unmanageable. Secondly, the control strategy lacks modularity. A small change in the system components may need expensive re-calibration of the control strategy. Thirdly, even in state-of-the-art EMS, the control algorithms neither exploit predictive driving information nor consider the coupling between the engine system and EATS, which leads to sudden NO_x emission peaks in the tailpipe during real-driving. As a result, heavy-duty vehicle industries are facing difficulties to meet progressively stringent real-driving NO_x (also called in-use or in-service) emission legislation.

One way of reducing the number of maps and sorting out dependencies is model-based development of control strategies. In general, model-based control strategies are developed for the diesel engine-EATS system, where the engine and EATS are optimized separately [7], [21]–[26]. Supervisory controllers are proposed in [27]–[29], where the solution of a single control problem optimizes the operation of both the engine and the EATS. Supervisory controllers have also been applied to hybrid electric vehicles and may control additional subsystems, such as waste heat recovery system [30]. All these supervisory control algorithms generate setpoints directly for the engine actuators, and the solutions of the formulated optimization problems are found by using Pontryagin's minimum principle (PMP) [31]. The Lagrangian multipliers of the Hamiltonian are calculated using heuristics and calibrated for world harmonized transient cycle (WHTC), i.e. the proposed algorithms do not guarantee optimal solutions for other drive cycles or real-driving.

This thesis work presents a supervisory control framework for an engine-EATS system, which focuses on overcoming limitations of previously proposed supervisory controllers, as well as limitations of existing control functionalities of EMS. The engine-EATS supervisor is part of an integrated powertrain control architecture, which has multiple hierarchical layers (vertically distributed control). The supervisory control layer receives engine torque and speed setpoint trajectories from higher-level control and provides optimized setpoint trajectories to the lower-level control. The diesel engine-EATS supervisor aims to reduce total consumption of

diesel fuel and AdBlue, and fulfil both the real-driving and WHTC cycle based NO_x emission legislation. The algorithms developed for the supervisor are verified and compared using a high-fidelity simulation platform, which includes a validated GT-POWER model of a 13 L turbo compound diesel engine and first-principles model of an EATS.

Thesis contributions

The significant contributions of the thesis in developing the engine-EATS supervisor are summarized below:

1. An optimal control problem (OCP) for the supervisor is formulated, which requires no change in the formulation if there is any change in the engine-EATS system.

2. The OCP is solved offline for a complete drive cycle, which minimizes total consumption of fuel and fulfils NO_x emission legislation for the cycle.

3. A mathematical model, required for real-driving emission control, is developed which predicts limits on accumulated tailpipe NO_x emission over a prediction horizon.

4. The OCP is also solved, in real-time, at every sampling instant of the E-NMPC based engine-EATS supervisor. The E-NMPC based supervisor explicitly controls real-driving and WHTC cycle based NO_x emission, and implicitly constraints PM emission. The algorithm does not require any heuristics or pre-calibration based on driving cycle.

5. An efficient version of the E-NMPC based supervisor is developed in C to integrate into the EMS. A dynamic link library (DLL) of the EMS software is also generated, for running software-in-the-loop (SIL) simulation.

Notation

The notation used in this thesis has up to four constituents: variable name, subscript, superscript, and accent mark. Variable names represent physical quantity, e.g., T (exhaust temperature [K]), μ (mass flow rate [kg/s]), m (mass [kg]), η (efficiency [-]), ω (angular speed [rad/s]), M (torque [N]), P (mechanical power [J/s]), and W (mechanical work [J]). In general, subscripts and superscripts use abbreviations, see Table 1.1,

Table 1.1: Subscripts or superscripts of used symbols

Subscripts		Superscripts	
E	in/after engine	f	fuel
tp	at tail pipe	exh	exhaust gas
SCR	in SCR	AB	AdBlue
		ss	steady-state

to represent physical location and chemical species, respectively. The type of variable is indicated using five accent marks: *check* (setpoint), *underline* (minimum), *overline* (maximum), *hat* (prediction), *dot* (derivative), and *tilde* (approximate). For example, engine-out NO_x mass flow rate setpoint is denoted $\check{u}_E^{NO_x}$.

Thesis outline

This thesis has two parts. Part I gives an overview of the complete work, and Part II contains research papers published related to the work. The organization of Part I is as follows. Chapter 2 describes real-driving emission legislation and provides a mathematical model which predicts limits on accumulated tailpipe NO_x emission over a prediction horizon. Chapter 3 explains the control model, which is required for the engine-EATS supervisor, along with the mathematical model developed in Chapter 2. This chapter also discusses the interface of the supervisor with an integrated powertrain control architecture and introduces the design and implementation of the supervisor. Chapter 4 implements the proposed engine-EATS supervisor for a specific powertrain and explains part of the results. Chapter 5 provides summaries of the included papers added in Part II. Finally, Chapter 6 concludes the overview part with suggested future work.

Real-driving Emission of NO_x

In heavy-duty diesel vehicles, emissions are tested during type approval and real-driving. During the type approval testing, the diesel vehicles cannot exceed the emission limits set for world harmonized stationary and transient cycle (WHSC and WHTC), and off-cycle emission (OCE). Real-driving emission testing requires field measurements, using a portable emissions measurement system (PEMS), conducted over urban roads, rural roads, and motorways. To handle the real-driving NO_x emission legislation in the supervisory controller, a mathematical model, which predicts allowed maximum emissions of NO_x over the prediction horizon, is developed as a part of this thesis work.

2.1 Real-driving emission legislation

During real-driving test, emissions are averaged over a moving work or CO_2 based window. The size of the window is the amount of engine-out work or CO_2 emission while driving the WHTC cycle during type approval testing of the same vehicle. In this work, averaging is done using the work-based-window (WBW). After starting the test based on WBW, PEMS begins to calculate the accumulated mechanical work and mass of emissions. When the accumulated work reaches a predefined window
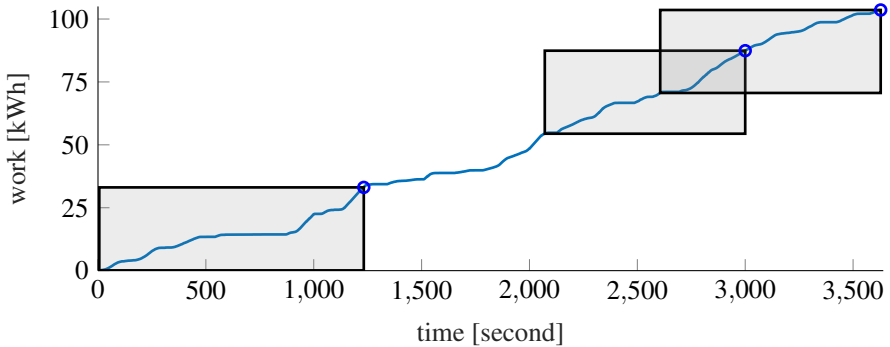
Figure 2.1: Few work-based-windows (WBWs) are plotted, which highlight that the size of the WBWs is constant in terms of accumulated work and different in time.

size for the first time, accumulated emissions over this window are calculated. After that, the calculation of the accumulated emissions over the moving window is carried out once every second. For Euro VI stage D and later [32], all accumulated emissions over the moving window must not exceed the maximum emission limits, excluding 10% of WBWs with the highest emission values. In addition, WBWs with the average power of less than 10% of the maximum power of the engine are not included in the evaluation.

Figure 2.1 provides an example to clarify the WBW concept. After driving 1232 s, accumulated work reaches 33 kWh. Here, 33 kWh is the size of the WBW for the engine used in this study. Hence, averaging of emissions over the moving window starts at 1232 s and continues once every second. The figure also shows that the size of the WBWs is constant in terms of accumulated work, but it varies with time.

2.2 NO$_x$ emission within a work-based-window

During the real-driving test, emissions over the last WBW are stored to calculate the average value of the emissions over the WBW. In an MPC setting, it is necessary also to predict allowed maximum emissions of NO$_x$ over the future WBWs using the stored NO$_x$ emissions over the last WBW. A mathematical model is developed below for this purpose.

Let the accumulated work variable W be defined as a function of time t as

$$W(t) = \int^t P(\tau)d\tau \quad \Rightarrow \quad \frac{d}{dt}W(t) = P(t), \tag{2.1}$$

where P is the instantaneous power delivered by the engine. Further, let the amount of accumulated mass of tailpipe NO$_x$ at time t be given by

$$m_{\text{tp}}^{\text{NO}_x}(t) = \int^t \mu_{\text{tp}}^{\text{NO}_x}(\tau)d\tau$$

where $\mu_{\text{tp}}^{\text{NO}_x}$ is the mass flow rate of tailpipe NO$_x$. Then the amount of emitted NO$_x$ within the most recent work-based-window, at time t, is given by

$$\Delta m_{\text{tp}}^{\text{NO}_x}(t) = \int_{t_0(t)}^t \mu_{\text{tp}}^{\text{NO}_x}(\tau)d\tau \tag{2.2}$$

where $[t_0(t), t]$ is the (varying) time window corresponding to the fixed mechanical work-based-window of size ΔW. The latter is implicitly defined by the relation

$$\int_{t_0(t)}^t P(\tau)d\tau = \Delta W. \tag{2.3}$$

Differentiating the two equations above gives

$$\frac{d}{dt}\Delta m_{\text{tp}}^{\text{NO}_x}(t) = \mu_{\text{tp}}^{\text{NO}_x}(t) - \mu_{\text{tp}}^{\text{NO}_x}(t_0)\frac{d}{dt}t_0(t) \tag{2.4}$$

$$P(t) - P(t_0)\frac{d}{dt}t_0(t) = 0 \tag{2.5}$$

which implies that the amount of emitted NO$_x$ over the sliding work-based-window is described by the 2nd order nonlinear state equation

$$\begin{cases} \dfrac{d}{dt}\Delta m_{\text{tp}}^{\text{NO}_x}(t) = \mu_{\text{tp}}^{\text{NO}_x}(t) - \mu_{\text{tp}}^{\text{NO}_x}(t_0)\dfrac{P(t)}{P(t_0)} \\ \\ \dfrac{d}{dt}t_0(t) = \dfrac{P(t)}{P(t_0)}, \end{cases} \tag{2.6}$$

where $\mu_{\text{tp}}^{\text{NO}_x}(\cdot)$ and $P(\cdot)$ act as exogenous signals that need to be stored in memory over $[t_0(t), t]$.

In papers B and C, a discretized version of the model 2.6 is used to estimate an

upper limit $\Delta\bar{m}_{tp}^{NO_x}$ on $\Delta m_{tp}^{NO_x}$ over a prediction horizon.

CHAPTER 3

Engine-EATS Supervisor

In general, each subsystem of vehicle powertrain and its respective control strategy is designed and optimized separately and assembled in the best possible ways. Nowadays, manufacturers are advancing towards integrated optimization of complete powertrain for better fuel efficiency, fulfilling progressively stringent emission legislation, and minimizing the vehicle production cost [33]. Systems and Control Division at the Chalmers University of Technology has proposed an integrated powertrain control architecture for a heavy-duty hybrid vehicle, and an engine-EATS supervisor is a part of it. This chapter discusses the interface of the engine-EATS supervisor with the integrated powertrain control architecture and then introduces the design and implementation of the engine-EATS supervisor.

3.1 Interface with existing control architecture

A heavy-duty diesel hybrid vehicle powertrain consists of a diesel engine, an EATS, an electric machine, an energy storage system (e.g. battery), and a transmission system. Considering the coupling among these powertrain subsystems and using predictive driving information for a very long horizon or entire route, designing a centralised integrated powertrain controller to operate all of the subsystems opti-
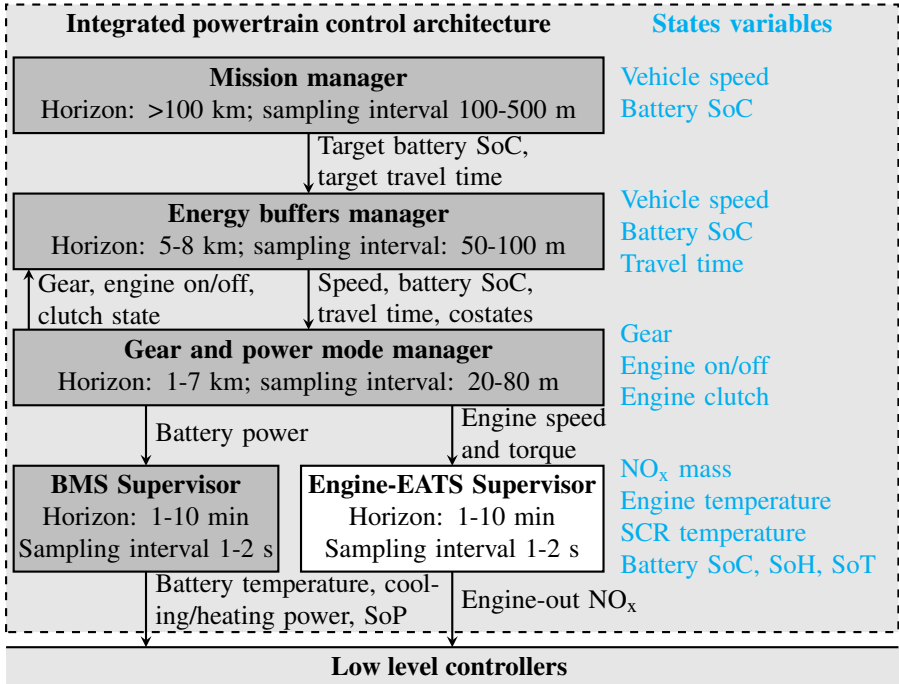
Integrated powertrain control architecture	States variables
Mission manager Horizon: >100 km; sampling interval 100-500 m	Vehicle speed Battery SoC
Target battery SoC, *target travel time*	
Energy buffers manager Horizon: 5-8 km; sampling interval: 50-100 m	Vehicle speed Battery SoC Travel time
Gear, engine on/off, clutch state Speed, battery SoC, travel time, costates	
Gear and power mode manager Horizon: 1-7 km; sampling interval: 20-80 m	Gear Engine on/off Engine clutch
Battery power Engine speed and torque	
BMS Supervisor Horizon: 1-10 min Sampling interval 1-2 s **Engine-EATS Supervisor** Horizon: 1-10 min Sampling interval 1-2 s	NO_x mass Engine temperature SCR temperature Battery SoC, SoH, SoT
Battery temperature, cool- ing/heating power, SoP Engine-out NO_x	
Low level controllers	

Figure 3.1: The schematic shows a hierarchical integrated powertrain control architecture. This thesis work focuses on the development of the engine-EATS supervisor, illustrated as the block with white background.

mally is impracticable. The hierarchical control architecture by Chalmers, shown in Figure 3.1, decomposes the integrated control problem into several sub-problems. It brings the benefit of using very long predictive driving information in terms of reduction in fuel consumption and fulfilling stringent emission legislation. This is named vertically distributed control architecture (multiple hierarchical layers) in the book [34]. In a vertically distributed control architecture, controllers in one level typically accept setpoints from higher levels and send setpoints to lower levels. The selection of control levels is typically based on time-scale separation. The time constant and time length of the prediction horizon gets shorter as we progress to lower levels. This type of vertical decomposition offers only sub-ordinations without enabling cooper-

ation among the different control units, i.e. communication is generally limited to one direction, from top to bottom.

The top three control layers of the hierarchical architecture in Figure 3.1 plan travel time, vehicle speed, battery state-of-charge (SoC), gear, and powertrain mode based on a highly abstracted powertrain model and predictive information of traffic, road topography and charging opportunities [35]–[39]. As outputs, these layers predict the forthcoming request of battery power, and engine speed and torque, which are then used as input trajectories to the fourth layer. The fourth control layer uses more detailed component models by incorporating thermal states. In this layer, a supervisor for the battery management system (BMS) and an E-NMPC based engine-EATS supervisor for the EMS work at the same time scale.

The engine-EATS supervisor is the focus of this thesis work. It receives engine torque and speed setpoint trajectories from higher-level controller along with current states of the engine-EATS system, e.g., engine-out temperature (T_E), SCR temperature (T_{SCR}), accumulated mass of tailpipe NO_x ($m_{tp}^{NO_x}$), and maximum achievable SCR NO_x conversion efficiency $\overline{\eta}_{SCR}^{NO_x}$. The output of the engine-EATS supervisor is optimal setpoint trajectories of engine-out NO_x mass flow rate ($\check{\mu}_E^{NO_x}$). A generic schematic of the interfaces of an engine-EATS supervisor with lower-level control, and its detailed version, are presented in Figure 3.2.

Figure 3.2 shows that the engine and the EATS, together with their respective control systems, are named *engine module* and *EATS module*, respectively. For both modules, the controllers have two cascaded loops with inner loop having actuators controllers (AC). The outer loop has an engine controller (EC) and an EATS controller (EAC) for the engine module and the EATS module, respectively. Both the *supervisory controller* (SC) and EC receive demanded engine torque and speed setpoints ($\check{M}_E$ and $\check{\omega}_E$) as input trajectories, coming from a higher-level controller. The goal of the supervisory controller is not tracking the input trajectories. Instead, it optimizes a cost function (obeying emission constraints) which is a direct reflection of the economy of the whole engine-EATS system and generates optimal $\check{\mu}_E^{NO_x}$ to the EC, considering the input trajectories as known disturbances. At the lower-level, EC consists of fuel and air-path controllers and tracks all three setpoint trajectories, including $\check{\mu}_E^{NO_x}$ trajectory, at sampling time 0.2 s, by providing setpoints to the actuators controllers of the engine module. The EAC does not track any setpoint from the higher-level. Instead, it always operates at maximum achievable SCR NO_x conversion efficiency $\overline{\eta}_{SCR}^{NO_x}$ and generates setpoints for the actuators controllers of the EATS module. The EATS module takes engine-out exhaust as a disturbance.
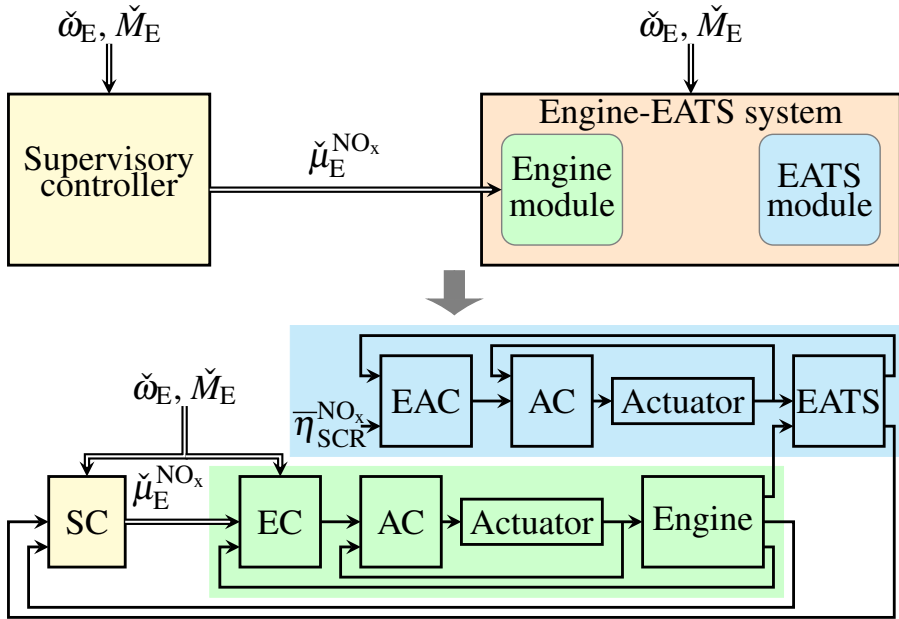
Figure 3.2: The upper block diagram shows a generic integrated control framework for the heavy-duty powertrain, consisting of a diesel engine and an exhaust aftertreatment system (EATS). The lower block diagram, indicated by the thick grey arrow, shows the detailed distributed control architecture of the engine-EATS system. Instantaneous signals are depicted by thin arrows, while double-line arrows indicate predicted trajectories.

3.2 Supervisory controller

The goal of this section is to introduce the design and implementation of a modular and EMS implementable supervisory controller which takes the benefit of using predictive driving information and considering the coupling between the engine system and EATS to reduce fuel consumption and fulfil emission legislation.

The previous section explains the interface of the engine-EATS supervisor with other layers. This section, firstly, provides a brief description of the control model used by the supervisor. Then, considering the coupling between the engine system and EATS, an optimal control problem is developed for reducing fuel consumption

and fulfiling emission legislation. Finally, the section explains the solution methods of the dynamic optimization problem. The detailed explanation of the design and real-time implementation of the engine-EATS supervisor is available in Paper C. As the engine-EATS supervisor coordinates both the engine system and EATS, it is also called integrated engine-EATS controller in the research papers.

Control model

The supervisory controller uses control models of the engine module and the EATS module, see Figure 3.3, and a mathematical model which predicts limits on $m_{tp}^{NO_x}$ over the prediction horizon in order to fulfil real-driving emission legislation, see Chapter 2. Development of the control model of the modules does not require much knowledge about the internal structure. The control model of the engine module has one input

$$u(t) = \check{\mu}_E^{NO_x}(t)$$

and two predicted disturbances

$$d(t) = [\check{\omega}_E(t), \check{M}_E(t)]^T.$$

Hence, there are in total three upper and lower bounded input signals to the engine module model. For a particular engine, input bounds $\overline{\omega}_E$ and $\underline{\omega}_E$ (overline and under-line mean upper and lower bound, respectively) are known parameters, and $\overline{M}_E(\check{\omega}_E)$
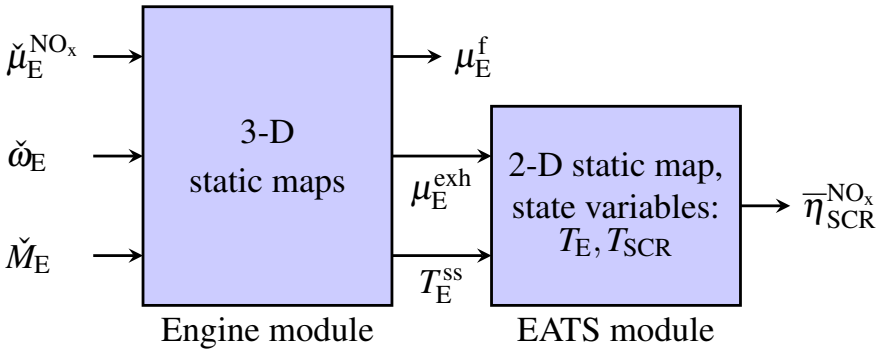

Figure 3.3: Control model of the engine and EATS modules.

and $\underline{M}_E(\breve{\omega}_E)$ are known 1-D look-up tables (static maps). The two remaining input bounds are developed, as a part of this thesis work, as 2-D maps, and these are $\bar{u}(d)$ and $\underline{u}(d)$. The engine module model also includes three output signals which are 3-D maps with independent variables u and d. These are engine diesel fuel mass flow rate $\mu_E^f(u,d)$, exhaust mass flow rate $\mu_E^{exh}(u,d)$, and engine-out exhaust steady-state temperature $T_E^{ss}(u,d)$. The control model of the EATS module takes the engine model outputs μ_E^{exh} and T_E^{ss} as inputs. A 2-D map provides $\overline{\eta}_{SCR}^{NO_x}$ as an output of the model. The map is a function of μ_E^{exh} and SCR temperature T_{SCR}. A second-order dynamic model with a time delay is developed for T_{SCR}, where state variables are T_E and T_{SCR}. The detailed mathematical model of the engine module and the EATS module are given in Paper C.

It is mentioned in Chapter 2 that, in an MPC setting, prediction of allowed maximum emissions of NO_x over the future WBWs is required. This prediction is used to define limits on $m_{tp}^{NO_x}$ over a prediction horizon. Hence, from the control design perspective, the manipulating variable u needs to have an influence on $m_{tp}^{NO_x}$. The nonlinear differential equation shows

$$\dot{m}_{tp}^{NO_x}(t) = \left(1 - \overline{\eta}_{SCR}^{NO_x}\left(\mu_E^{exh}(u,d), T_{SCR}\right)\right) u(t) \tag{3.1}$$

the influence of u on $m_{tp}^{NO_x}$ given that d is known. The $\overline{\eta}_{SCR}^{NO_x}$ is defined by the equation

$$\overline{\eta}_{SCR}^{NO_x} = \frac{\mu_E^{NO_x} - \mu_{tp}^{NO_x}}{\mu_E^{NO_x}},$$

but it is approximately modelled as a 2-D map $\overline{\eta}_{SCR}^{NO_x}\left(\mu_E^{exh}(u,d), T_{SCR}\right)$ for prediction.

Problem formulation

The objective of the supervisory controller is to minimize the total cost of diesel fuel and AdBlue subject to the input constraints, a state constraint, and differential equations. A descriptive optimal control problem for the supervisor is formulated as follows:

$$\min_{u(\cdot)} \quad \text{total cost of diesel fuel and AdBlue} \tag{3.2a}$$

subject to:

SCR temperature dynamics $\hphantom{xxxxxxxxxxxxxxxxxxxxxxxxxxxxx}$ (3.2b)

$$\dot{m}_{\text{tp}}^{\text{NO}_{\text{x}}}(t) = \left(1 - \overline{\eta}_{\text{SCR}}^{\text{NO}_{\text{x}}}\big(\mu_{\text{E}}^{\text{exh}}(u,d), T_{\text{SCR}} \big) \right) u(t) \tag{3.2c}$$

$$\text{state constraint on } m_{\text{tp}}^{\text{NO}_{\text{x}}}(t) \tag{3.2d}$$

$$\text{input constraints } \overline{u}(d) \text{ and } \underline{u}(d) \tag{3.2e}$$

$$\text{initial condition of dynamic states.} \tag{3.2f}$$

At every controller sampling instant, the E-NMPC based supervisor needs to solve the optimization problem (3.2) for a look-ahead horizon of $2-8\,$min. The optimization problem contains three 2-D and three 3-D maps. While solving the optimization problem, an additional computationally efficient algorithm is required for interpolating the maps. The state constraint (3.2d) is calculated in real-time for the same look-ahead horizon using the mathematical model described in Chapter 2. The two other states T_{E} and T_{SCR}, describing SCR temperature dynamics, are unconstrained.

Optimisation methods

The problem (3.2) is a continuous-time, nonlinear, and non-convex optimal control problem including 2-D and 3-D maps. There is no closed-form solution to the problem. Obtaining a computationally efficient numerical solution of the problem is also complicated: a compromise needs to be made between computation time and accuracy while choosing a numerical optimization method and during the implementation of it. Three possible numerical optimization methods are dynamic programming (DP), direct optimal control (DOC), and Pontryagin's minimum principle (PMP).

For DP and DOC approaches, the optimization problem is discretized first and then solved. The DP approach provides a globally optimal solution. But, solving an optimal control problem with three states, one control input, state and input constraints, and 2-D and 3-D maps for the prediction horizon of $100-500$ samples ($2-8\,$min with controller sampling time $1\,$sec) is computationally impractical for real-time implementation. The DOC approach solves the discretized optimal control problem with nonlinear optimization algorithms, e.g. interior-point and sequential quadratic programming (SQP), and provides a locally optimal solution.

PMP method finds continuous-time equations describing the solution to the optimization problem in continuous-time. Then, the continuous-time equations are discretized, and a locally optimal solution is found using numerical methods. For the PMP method, handling state constraints is much harder. Papers B and C reformulate the optimization problem so that the PMP method is applicable in a computationally efficient manner.

2-D and 3-D maps

The data generation method for the 2-D and 3-D maps using hi-fidelity simulation platform, how the generated data are stored in the EMS to reduce the memory requirement, and the interpolation algorithm used during optimization are explained in Paper C. The 2-D map $\overline{\eta}_{\mathrm{SCR}}^{\mathrm{NO_x}}(\mu_{\mathrm{E}}^{\mathrm{exh}}, T_{\mathrm{SCR}})$ is always stored as gridded data. Two different approaches are used for handling the 3-D and remaining 2-D maps. One approach stores all of these maps as scattered data and uses real-time scattered linear interpolation (SLI) algorithm for interpolating the maps. This version of the supervisory controller is named as SC-SLI. Another version approximates the 3-D maps with functions and stores the coefficients of the functions in the memory. The supervisory controller with function approximation of the 3-D maps is named as SC-FAM. The SC-FAM stores the remaining 2-D maps as scattered data and uses real-time SLI algorithm for interpolation. The detailed description and comparison of these two versions of the supervisor are available in Paper C.

Case Study

The engine-EATS supervisor in Chapter 3 is applicable for a wide variety of vehicle powertrains. In this chapter, the supervisory controller is applied to a long haul heavy-duty engine-EATS system with a 13 L six-cylinder turbo-compound diesel engine.

4.1 System description

The engine-EATS system used for this case study is shown in Figure 4.1. The engine system comprises several components, including a 13 L six-cylinder diesel engine, air filter, charge-air cooler, an intake throttle valve (ITV), exhaust gas recirculation (EGR) system, mixer, turbo compound (TC), and fuel injection system. The EATS consists of three components: diesel oxidation catalyst (DOC), diesel particulate filter (DPF), and selective catalytic reduction (SCR) including ammonia slip catalyst (ASC). In the following, the most important characteristics of the subsystems and actuators are explained.

The engine fuel controller uses demanded engine speed and torque to calculate diesel fuel flow rate. Engine-out NO_x mass flow rate setpoint from the higher-level control is used for fuel injection timing and multiple fuel injection. Delayed fuel
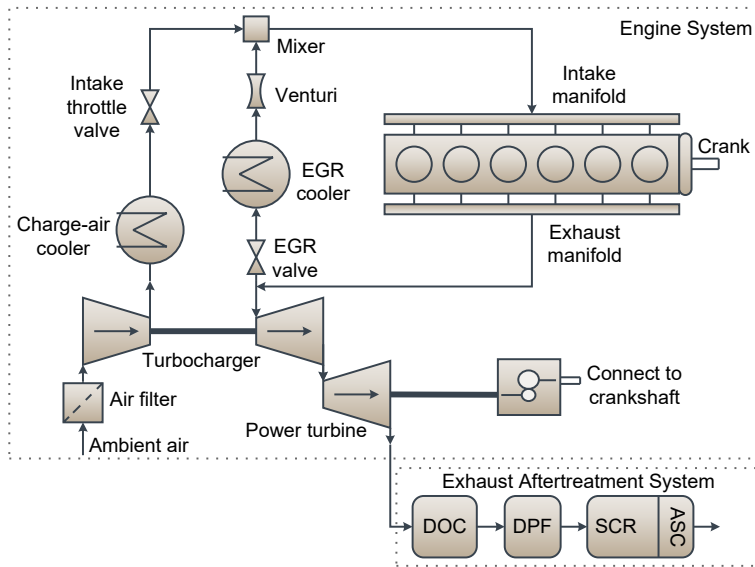
Figure 4.1: Schematic representation shows a long haul heavy-duty powertrain. The engine system has an air filter, charge-air cooler (CAC), intake throttle valve (ITV), exhaust gas recirculation (EGR) system, mixer, and turbo compound (TC). The exhaust aftertreatment system (EATS) consists of a diesel oxidation catalyst (DOC), a diesel particulate filter (DPF), and a selective catalytic reduction (SCR) including ammonia slip catalyst (ASC).

injection means less NO_x and more unburned fuel (i.e. reduced fuel efficiency, more PM, and more HC); and multiple fuel injection reduces engine sound and all types of emissions. The MPC based engine air-path controller takes engine-out NO_x mass flow rate as setpoint from the supervisor, and engine speed and diesel fuel flow rate as disturbances. The air-path controller uses the ITV position and the EGR valve position as manipulating variables to minimize fuel consumption, fulfil emission constraints, and maximize exhaust thermal power under certain conditions.

The EGR system is used to recirculate a fraction of the exhaust gas back to the combustion chamber for primarily reducing NO_x emission from the engine. It consists of an EGR cooler, an EGR valve, and a venturi. The EGR cooler is used for

cooling down the recirculated exhaust gas to maintain a lower temperature of charged air, a mix of fresh air and cooled exhaust gas. Extra exhaust gas in the charged air absorbs part of the heat energy. Therefore, recirculated exhaust gas decreases peak combustion temperature, leading to reduced NO_x emissions. The EGR valve controller tracks the EGR valve position setpoint from the air-path controller to regulate the exhaust flow rate through the EGR system. The venturi measures the exhaust flow rate through the EGR system.

The ITV is used to control exhaust temperature by controlling air intake to the cylinders. Demanded power of the engine is delivered by controlling the fuel flow. Hence, the air-fuel ratio increases with the decrease of demanded power, if air intake to the cylinders does not decrease in the same proportion. The result of the increased air-fuel ratio is the decrease in engine exhaust temperature. Thus, at low power, ITV can be controlled to decrease air intake to the cylinders and eventually increase the exhaust temperature whenever required. Similarly, ITV can also be controlled to decrease the exhaust temperature at high power demand. ITV response should be fast enough to handle rapid changes in demanded power. In [40], ITV is used to increase the engine exhaust temperature for regeneration of the particulate filter. Different methods of controlling exhaust temperature are discussed in [41].

The TC includes a power turbine, connected in series with a traditional turbocharger, and an advanced gear train. The power turbine re-uses exhaust gases (containing 20-25% of total fuel energy) from the turbocharger and provides recovered 5% of the total fuel energy to the crankshaft via the advanced gear train [42]. The power turbine increases exhaust back pressure leading to increased pumping loss. Thus, considering the increased pumping loss for long haul applications, TC can add an additional 3% of the total fuel energy to the crankshaft via an advanced gear train. Further information on the TC diesel engine can be found in [43].

The EATS connects DOC, DPF, SCR, and ASC in cascade, as shown in Figure 4.1. In the presence of oxygen, DOC converts CO and HC into CO_2 and water through oxidation using palladium or/and platinum catalysts with about 90% efficiency. The DOC also oxidizes NO into NO_2, which is good both for DPF and SCR. The DPF accumulates PM and burns it through passive and active regeneration with about $80 - 100\%$ efficiency. At $300 - 450\,°C$ temperature inside the DPF, NO_2 oxidizes the accumulated PM into CO_2 and water which is called passive regeneration. A differential pressure sensor estimates the accumulated PM in the DPF. If the amount of PM exceeds a predefined limit, it triggers the EMS to raise the exhaust temperature, about $600\,°C$, for active regeneration. For increasing the exhaust temperature, fuel is

23

added with the exhaust gas either by injecting fuel during the exhaust stroke of the engine or using an additional injector before the DOC. The DOC acts as a catalyst for burning the added fuel. When the engine operates at high power region, higher exhaust temperature can also cause self-regeneration of the DPF. An aqueous urea solution, known as diesel exhaust fluid (DEF) or AdBlue, is injected to the SCR inlet to reduce NO_x from the exhaust. After vaporization of the aqueous solution, the urea decomposes into NH_3. The NH_3 reacts with NO_x and mainly produces Nitrogen and water. The higher concentration of NH_3 increases the SCR NO_x conversion efficiency, but it also can increase the amount of NH_3 released out of the SCR. The ASC is used to decrease the NH_3 slip. The NO_x conversion efficiency of SCR also depends on NO_2 fraction (defined as the ratio NO_2/NO_x). The higher NO_2 fraction, obtained by DOC, means increased SCR NO_x conversion efficiency.

4.2 Development of supervisory controller

Based on the knowledge gathered from the system studies and simulation results, the OCP developed for the engine-EATS supervisor is decomposed into two, much simpler, sub-problems. The *setpoint generator* and *SCR temperature predictor* blocks,
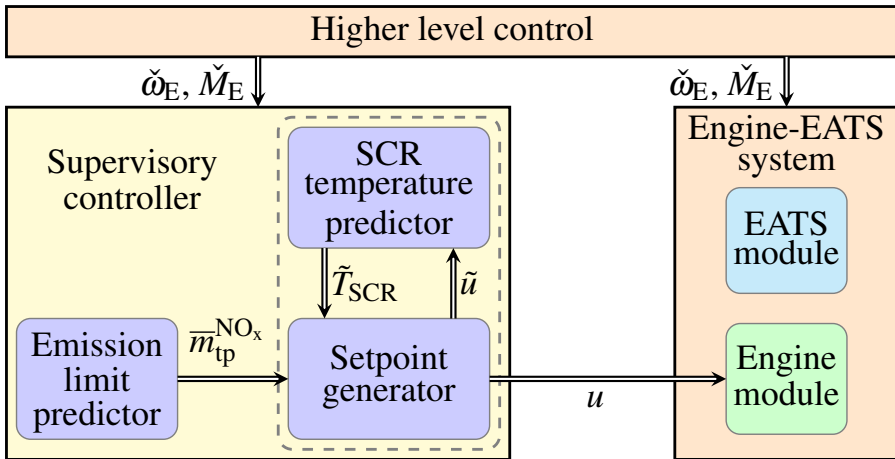

Figure 4.2: Block diagram highlights the three coordinated functionalities of the supervisory controller.
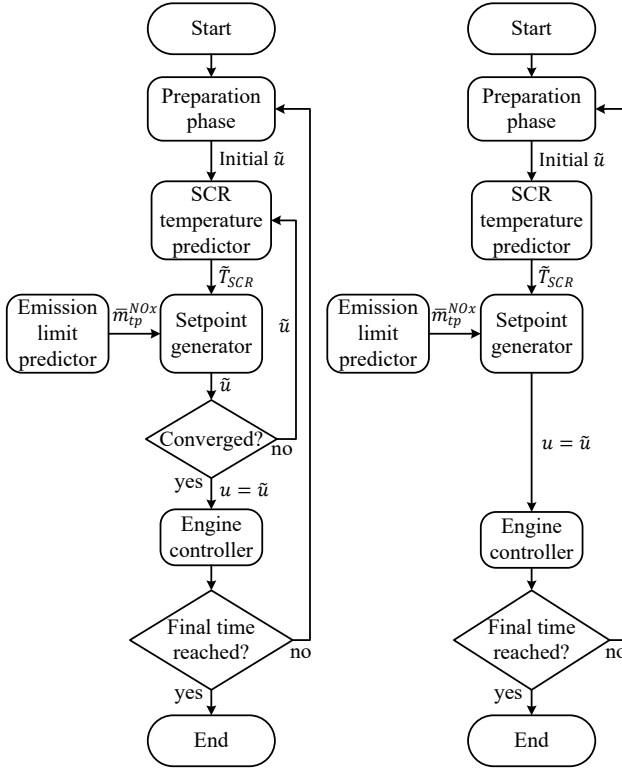
Figure 4.3: Flow-chart of E-NMPC based supervisory control algorithm: without RTI (left) and with RTI (right).

see Figure 4.2, individually solve the two sub-problems. The two blocks iteratively solve the original OCP using updated limits on $m_{tp}^{NO_x}$, from another block called *emission limits predictor* which uses the model developed in Chapter 2.

The iterative procedure is started with an initial guess of the control input trajectory. Then, the SCR temperature predictor uses the initial guess to simulate the temperature dynamics for calculating $\tilde{T}_{SCR}$. After that, $\tilde{T}_{SCR}$ is shared with the setpoint generator, which solves an optimization problem using the PMP method to generate $\tilde{u}$. The iteration continues until $\tilde{u}$ converges to optimal u, see left flow chart in Figure 4.3. Numerical results are analyzed in Papers B and C to illustrate that

the distributed optimization strategy works. It is shown in the papers that the solution converges to the optimal one within four iterations when initialized with a pre-calibrated map. The map is generated by offline calibration.

This iterative optimization algorithm solves the OCP at every sampling instant of the E-NMPC based supervisor. In the case of E-NMPC, only the first optimal solution, for a prediction length of N samples, is found with initial guess calculated using the pre-calibrated map. Later on, an initial guess of input trajectory is found by left shifting the previous optimal input trajectory, where the last sample still comes from the pre-calibrated map. With this warm-start, only one iteration between the setpoint generator and SCR temperature predictor is showed to be enough for getting the optimal solution, see the right flow chart in Figure 4.3. This technique is called real-time iteration (RTI) [44].

4.3 Results

Two different versions of the E-NMPC based supervisory control algorithm, SC-SLI and SC-FAM, are explained in Papers B and C. This section presents the results for the SC-FAM, which approximates the 3-D maps with functions to improve the computational efficiency and memory use.

The results are found using a high-fidelity simulation platform. The platform consists of the supervisory controller, and the engine and EATS modules, see Figure 4.2. The development of the high-level controller depicted in the figure is outside the scope of this thesis. Instead, the demanded speed and torque trajectories are calculated offline for two different cycles—WHTC cycle and another measured cycle—for a 13 L turbo compound diesel engine used in this work. The measured cycle is recorded by driving a heavy-duty truck from Borås to Landvetter to Borås in the Gothenburg area, Sweden, called BLB cycle. Figure 4.4 shows the demanded speed and torque trajectories estimated, for the engine used in this case study, from the WHTC and BLB cycles. The WHTC cycle is used to show that the algorithm fulfils the WHTC cycle based emission legislation, and the BLB cycle is used for detailed validation of the algorithm.

The SC-FAM algorithm is developed in three different variants: without RTI, with RTI, and with RTIb (RTI with bounded costate). For SC-FAM without RTI, four iterations between the setpoint generator and SCR temperature predictor are generally sufficient for convergence. At every iteration, both $\tilde{T}_{\mathrm{SCR}}$ and $\tilde{u}$ are updated, with 75% step size. The SC-FAM with RTI does the job with only one iteration and updates

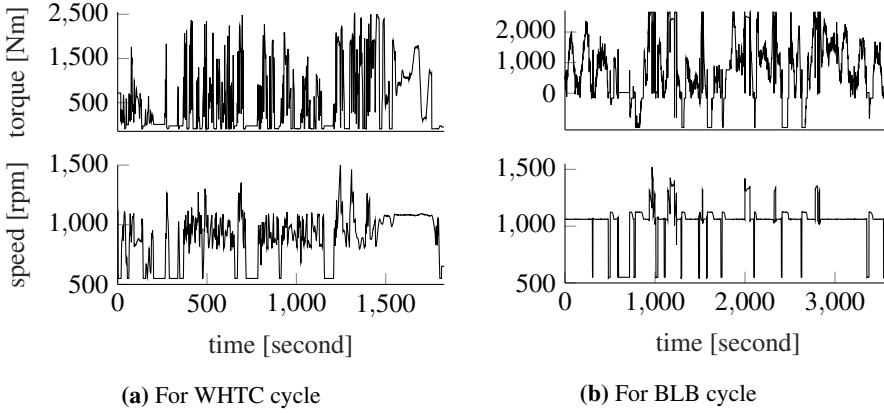**(a)** For WHTC cycle   **(b)** For BLB cycle

Figure 4.4: Speed and torque trajectories estimated from the world harmonized transient cycle (WHTC) and Borås-Landvetter-Borås (BLB) cycles.
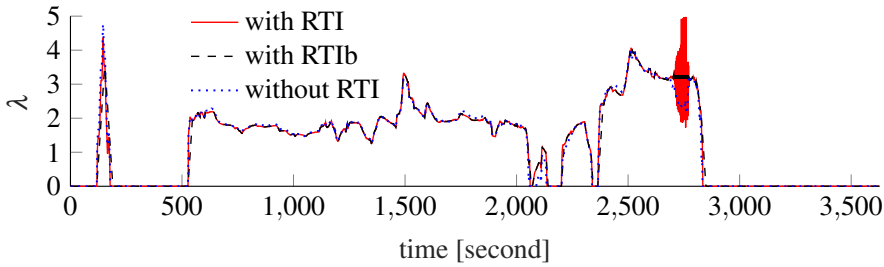

Figure 4.5: The plot shows the optimal Lagrangian multipliers of the Hamiltonian (costate) λ while the simplified optimization problem in the setpoint generator is solved.

both $\tilde{T}_{\text{SCR}}$ and $\tilde{u}$ with 75% step size. The SC-FAM with RTIb does everything same as the last one but limits the change in costate λ within 0.1 (while solving the optimization problem formulated for the setpoint generator) from the previous sampling instant to the current sampling instant of the supervisory controller.

Figure 4.5 shows optimal costate λ when the simulation is carried out for the three different variations of the SC-FAM algorithm with the BLB cycle. For the SC-FAM without RTI, λ always reaches the optimal value. For a few cases, like in the
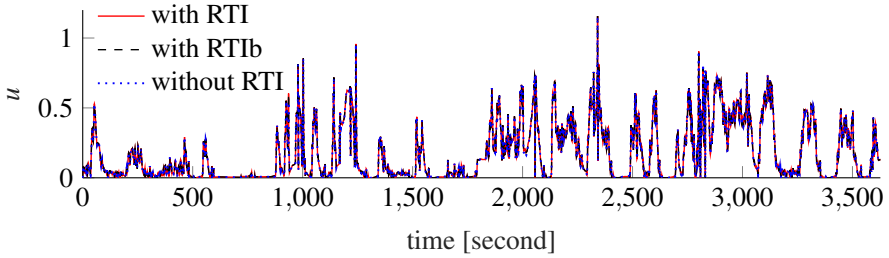
27

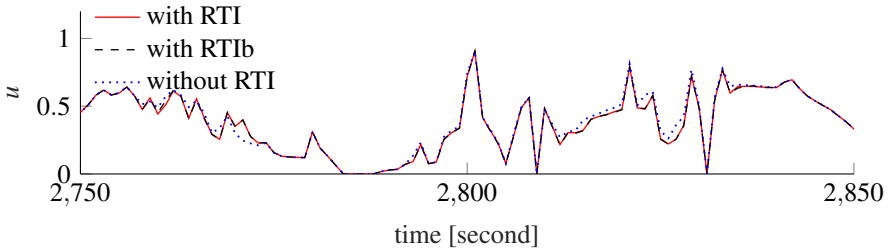**Figure 4.6:** Optimal trajectory of normalized input *u*

Figure 4.7: Optimal trajectory of normalized input *u* (zoomed)

Figure 4.5, λ may have oscillation for the SC-FAM with RTI. But, the corresponding optimal input trajectory in 4.6 does not show a significant difference with SC-FAM without RTI. The three input trajectories are plotted in Figure 4.7 for the period when λ has oscillation. Moreover, delivered energy, fuel consumption, tail-pipe NO_x, and NH_3 slip are same for both cases. To avoid the oscillation in λ, the SC-FAM with RTIb limits the change in λ.

The SC-FAM with RTIb is selected for implementation in the EMS considering the computation time and accuracy. The E-NMPC based supervisor with RTIb is compared for four different prediction horizon length $N = [100, 200, 300, 400]$. Figure 4.8 depicts the emission over work-based-window (WBW) when the total fuel consumption is almost the same for the four cases. The empty portion of the WBW NO_x emission plot is because the accumulated work reaches the predefined window size of 33 kWh at 1256 s for the first time. The figure shows that WBW NO_x emission is well below 0.46 g/kWh for all cases. The plot also has a few areas, where
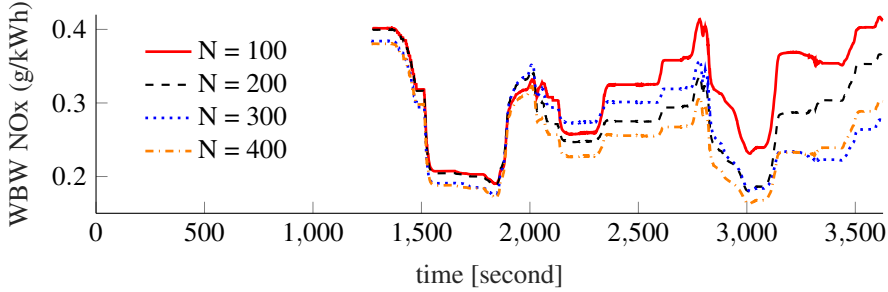
Figure 4.8: Real-time emission over work-based-window (WBW) with different horizon length in sample.

Table 4.1: Comparing SC-FAM with RTIb for different prediction horizon

Horizon	BSTN [g/kWh]	90th percentile of WBW NO_x [g/kWh]
$N = 100$	0.3763	0.4015
$N = 200$	0.3417	0.3530
$N = 300$	0.3153	0.3414
$N = 400$	0.3083	0.3103

emission is far below the limit. These are because the algorithms fulfil both Euro VI real-driving and WHTC cycle based NO_x emission legislation. The WHTC cycle based NO_x emission limit is 0.46 g/kWh, but a conformity factor of 1.5 applies to real-driving emission testing. If the supervisory controller predicts that any of the emission limits are going to be violated, then it decreases the emission at the cost of extra fuel. What is more, the supervisor never tries to decrease the AdBlue injection to increase the emissions. Table 4.1 compares the algorithm for different prediction horizons in terms of break specific tailpipe NO_x (BSTN) and 90th percentile of WBW NO_x when the break specific total consumption (BSTC) is almost the same for all cases. The table shows that both BSTN and 90th percentile of WBW NO_x decrease with the increase in the prediction length.

The results of the E-NMPC based supervisor are compared with a baseline controller where OCP is solved offline for complete BLB cycle. The upper plot of the Figure 4.9 shows BSTN and 90th percentile of WBW NO_x for the baseline controller
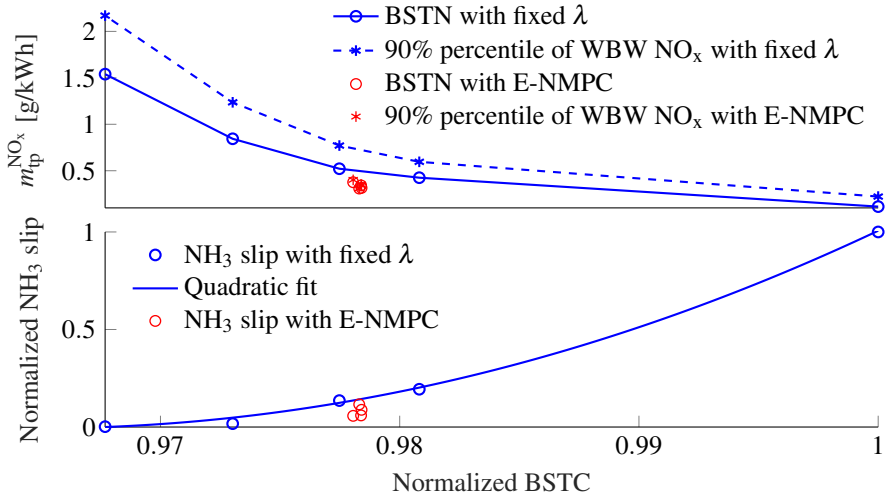
Figure 4.9: $m_{tp}^{NO_x}$ and NH_3 slip versus break specific total consumption (BSTC)

optimized for five different tailpipe NO_x constraints. Both BSTN and 90th percentile of WBW NO_x decrease with the increase of BSTC. The important observation here is that both BSTN and 90th percentile of WBW NO_x from the E-NMPC based supervisor are significantly lower than those from the baseline controller. What is more, the lower plot shows that NH_3 slip from the E-NMPC based supervisor is also significantly lower than that from the baseline controller. Simulation results show that the supervisory controller, with prediction length 400 samples, has 1.7% less total fuel consumption and 88.4% less NH_3 slip, compared to the baseline controller, to achieve the same real-driving NO_x emission. In other words, the baseline controller can achieve the same 90th percentile of WBW NO_x, like the E-NMPC based supervisor having prediction length 400 samples, with an increase of 1.8% fuel consumption and 555% NH_3 slip.

30

Summary of included papers

This chapter provides a summary of the included papers.

5.1 Paper A

Mohammed R. Karim, Nikolce Murgovski, Esteban R. Gelso, and Bo Egardt
Supervisory Framework and Model-based Control of Engine and Exhaust Aftertreatment System
Limassol, Cyprus, June 12-15, 2018.

The paper proposes a supervisory control framework for a heavy-duty diesel engine-EATS system. The OCP developed for the supervisory controller requires no change in the problem formulation if there is any change in the engine-EATS system, and minimizes the total consumption of fuel while fulfilling Euro VI NO_x emission legislation. The formulated OCP is highly nonlinear and non-convex. For a computationally efficient solution, the OCP is decomposed into two much simpler sub-problems which are individually solved by the setpoint generator and the EATS setpoint generator. The two blocks take an average NO_x emission limit, for a complete drive

cycle, from the emission limits generator and iteratively find the offline solution of the original OCP, see contributions 1 and 2. The paper provides a detail explanation of the engine setpoint generator. In this block, a simplified OCP is solved by dynamic programming (DP) as a benchmark and Pontryagin's minimum principle as a computationally efficient algorithm. Results obtained by using both methods show no significant differences in terms of total fuel consumption and emission. The developed supervisor has less number of maps and manually tunable parameters compared to a standard controller used in the industry consisting of feed-forward maps and feedback control. Simulation results show 0.5% decrease in total fuel consumption, compared to the standard controller, while maintaining NO_x emissions under the legislative limit.

5.2 Paper B

Mohammed R. Karim, Bo Egardt, Nikolce Murgovski, and Esteban R. Gelso
Supervisory Control for Real-Driving Emission Compliance of Heavy-Duty Vehicles
IFAC-PapersOnLine,
Volume 51, Issue 31, 2018, Pages 460-466
©2020 Elsevier B.V. DOI: 10.1016/j.ifacol.2018.10.103 .

This paper updates the supervisory control framework, for a heavy-duty diesel engine-EATS system, proposed in Paper A. The updated control framework fulfils Euro VI real-driving NO_x emission legislation in addition to the features of the previous version. The new framework has three function blocks: setpoint generator, SCR temperature predictor, and emission limits predictor. A developed mathematical model is used by the emission limits predictor for predicting limits on accumulated tailpipe NO_x emission over the prediction horizon. The formulated OCP is horizontally decomposed into two sub-problems which are individually solved by the setpoint generator and the SCR temperature predictor. The two blocks iteratively solve the original OCP, using updated limits from the emission limits predictor, at every sampling instant of the E-NMPC based supervisor, see contributions 1, 3 and 4. The paper validates the supervisory controller using a high-fidelity simulation platform including a validated GT-POWER model of a 13 L turbo compound diesel engine and a first-principles model of an EATS. Simulation results show that the strategy always fulfils the real-driving emission legislation.

5.3 Paper C

Mohammed R. Karim, Bo Egardt, Esteban R. Gelso, and Nikolce Murgovski
Supervisory Control for NO_x Emission Compliance of Heavy-Duty Vehicles
IEEE Transactions on Vehicular Technology .

This article provides a detailed description of the supervisory control framework proposed for any heavy-duty vehicles consisting of a diesel engine and an exhaust aftertreatment system (EATS). The engine-EATS supervisor is based on distributed E-NMPC which fulfils both the Euro VI real-driving and WHTC cycle based NO_x emission legislation. The article also compares the results found from two different versions of the engine-EATS supervisor using the high-fidelity simulation platform. One is an updated version of the algorithm presented in Paper B, and another is a newly developed computationally more efficient algorithm. The processing capacity of the existing production EMS is considered while designing the new version, and finally, this is developed in C as an EMS software. A dynamic link library of the EMS software is also generated for running software-in-the-loop simulation, see contributions 4 and 5.

CHAPTER 6

Concluding Remarks and Future Work

This thesis develops and evaluates an engine-EATS supervisor, which is a part of an integrated powertrain control architecture aimed for heavy-duty vehicles. This chapter highlights a few important properties of the supervisor and then discusses the scope of future work.

In existing EMS, understanding the dependencies between functionalities is hard and finding out the effect of a newly added functionality to other functionalities is harder. To overcome this difficulty, the engine system and EATS as well as their corresponding control functionalities are encapsulated within the engine module and EATS module, respectively. Each module can have limited and understandable interaction with other modules and with the supervisory controller. What is more, the setpoint generated by the supervisory controller is a common signal in all engine system configurations, which makes the supervisory control problem formulation independent of the engine systems. Any change inside the engine or EATS module does not require reformulation of the control problem at the supervisory level. The chosen setpoint also reduces the dimension of the supervisory control problem, which decreases computation time, memory use, and complexity of the algorithm.

The engine and EATS modules are highly coupled. For example, the EATS is affected by the engine exhaust characteristics (temperature and flow rates of the main

species). The developed E-NMPC based engine-EATS supervisor considers the coupling while taking control decision, which results in reduced total fuel consumption and fulfilling both the real-driving and WHTC cycle based NO_x emission legislation. The EATS is always operated at maximum achievable NO_x conversion efficiency, i.e., the supervisor never tries to decrease the AdBlue injection to increase the emissions.

The formulated OCP is a nonlinear and non-convex dynamic optimization problem with one control signal and three state variables. For developing a computationally efficient E-NMPC based supervisory control algorithm, with look-ahead horizon $2-8$ min, two simplifications are made in the original OCP, see the Paper B and C. With an improved initialization technique, real-time iteration of the E-NMPC based supervisor is showed enough for getting the optimal solution, see Paper C.

This thesis work does not find a solution to the original OCP, because solving a highly nonlinear and non-convex OCP over a long prediction horizon is computationally demanding. Comparison of the solution to the original OCP with the current one would be important future work to see how much could be gained if more computation power is available. The control model used in the OCP is simple. A more accurate control model of the EATS module might provide better results. The OCP developed for the supervisor may also consider explicit control of NH_3 slip and uncertainty in the prediction of engine speed and torque.

Most of the tailpipe NO_x emission happens when SCR temperature is low, but the engine operates at high power. To further reduce the tailpipe NO_x, the SCR can be heated up during this condition (especially after the long operation at low power when the engine switches to high power). This heating up problem can be added to the current OCP which only controls engine-out NO_x during this situation.

References

[1]   I. T. Forum, *ITF Transport Outlook 2019*. 2019.

[2]   M. Zheng, G. T. Readerb, and J. G. Hawley, "Diesel engine exhaust gas re-circulation –- a review on advanced and novel concepts", *Energy Conversion and Management*, vol. 45, no. 6, pp. 883–900, Apr. 2004.

[3]   Y. Zhao, K. Cui, J. Zhu, S. Chen, *et al.*, "Effects of retarding fuel injection timing on toxic organic pollutant emissions from diesel engines", *Aerosol and Air Quality Research*, vol. 19, no. 6, pp. 1346–1354, 2019.

[4]   S. Jaichandar and K. Annamalai, "Combined impact of injection pressure and combustion chamber geometry on the performance of a biodiesel fueled diesel engine", *Energy*, vol. 55, pp. 330–339, Jun. 2013.

[5]   K. V. Tanin, D. D. Wickman, D. T. Montgomery, S. Das, and R. D. Reitz, "The influence of boost pressure on emissions and fuel consumption of a heavy-duty single-cylinder d.i. diesel engine", SAE International, Technical Paper 1999-01-0840, Jan. 1999.

[6]   B. Mohan, W. Yang, and S. kiang Chou, "Fuel injection strategies for performance improvement and emissions reduction in compression ignition engines—a review", *Renewable and Sustainable Energy Reviews*, vol. 28, pp. 664–676, 2013.

[7]   C. M. Schär, C. H. Onder, and H. P. Geering, "Control of an SCR catalytic converter system for a mobile heavy-duty application", *IEEE Trans. Contr. Syst. Technol.*, vol. 14, no. 4, pp. 641–653, Jul. 2006.

[8]   N. Watson and M. S. Janota, *Turbocharging the internal combustion engine*. The Macmillan Press Ltd, 1982.

[9]   M. Åhman, "Primary energy efficiency of alternative powertrains in vehicles", *Energy*, vol. 26, pp. 973–989, 11 Nov. 2001.

[10] S. Kobayashi, S. Plotkin, and S. K. Ribeiro, "Energy efficiency technologies for road vehicles", *Energy efficiency*, vol. 2, pp. 125–137, 2 May 2009.

[11] H. K. Roy, A. McGordon, and P. A. Jennings, "A generalized powertrain design optimization methodology to reduce fuel economy variability in hybrid electric vehicles", *IEEE Trans. Veh. Technol*, vol. 63, no. 3, pp. 1055–1070, Mar. 2014.

[12] F. R. Yu, "Connected vehicles for intelligent transportation systems", *IEEE Trans. Veh. Technol*, vol. 65, no. 6, pp. 3843–3844, Jun. 2016.

[13] D. A. do Nascimento, Y. Iano, *et al.*, "Sustainable adoption of connected vehicles in the brazilian landscape: Policies, technical specifications and challenges", *Transactions on Environment and Electrical Engineering*, vol. 3, no. 1, pp. 44–62, Mar. 2019.

[14] G. Descornet, *Road-Surface Influence on Tire Rolling Resistance.* In STP1031-EB Surface Characteristics of Roadways: International Research, Technologies, edited by Meyer, W., and Reichert, J., (pp. 415-1990). West Conshohocken, PA: ASTM International, 10.1520/STP23377S, 1990.

[15] L. Johannesson, N. Murgovski, E. Jonasson, J. Hellgren, and B. Egardt, "Predictive energy management of hybrid long-haul trucks", *Control Engineering Practice*, vol. 41, pp. 83–97, 2015.

[16] L. Deng, M. H. Hajiesmaili, M. Chen, and H. Zeng, "Energy-efficient timely transportation of long-haul heavy-duty trucks", *IEEE Transactions on Intelligent Transportation Systems*, vol. 19, no. 7, pp. 2099–2113, 2018.

[17] T. Hlasny, M. P. Fanti, A. M. Mangini, G. Rotunno, and B. Turchiano, "Optimal fuel consumption for heavy trucks: A review", in *2017 IEEE International Conference on Service Operations and Logistics, and Informatics (SOLI)*, 2017, pp. 80–85.

[18] A. A. Alam, A. Gattami, and K. H. Johansson, "An experimental study on the fuel reduction potential of heavy duty vehicle platooning", in *13th International IEEE Conference on Intelligent Transportation Systems*, 2010, pp. 306–311.

[19] U. Montanaro, S. Dixit, S. Fallah, M. Dianati, A. Stevens, D. Oxtoby, and A. Mouzakitis, "Towards connected autonomous driving: Review of use-cases", *Vehicle System Dynamics*, vol. 57, no. 6, pp. 779–814, 2019.

[20] L. Eriksson and L. Nielsen, "Engine management systems—an introduction", in *Modeling and Control of Engines and Drivelines*. John Wiley & Sons, Ltd, 2014, ch. 9, pp. 263–270.

[21] L. Guzzella and A. Amstutz, "Control of diesel engines", *IEEE Control Syst. Mag.*, vol. 18, no. 5, pp. 53–71, Oct. 1998.

[22] J. Rückert, A. Schloßer, H. Rake, B. Kinoo, M. Krüger, and S. Pischingert, "Model based boost pressure and exhaust gas recirculation rate control for a diesel engine with variable turbine geometry", *IFAC Proceedings Volumes*, vol. 34, no. 1, pp. 277–282, 2001, 3rd IFAC Workshop on Advances in Automotive Control 2001, Karlsruhe, Germany, 28-30 March 2001.

[23] M. Devarakonda, G. Parker, J. H. Johnson, and V. Strots, "Model-based control system design in a urea-scr aftertreatment system based on nh3 sensor feedback", *International Journal of Automotive Technology*, vol. 10, no. 6, pp. 1976–3832, 2009.

[24] J. Wahlström, L. Eriksson, and L. Nielsen, "Egr-vgt control and tuning for pumping work minimization and emission control", *IEEE Transactions on Control Systems Technology*, vol. 18, no. 4, pp. 993–1003, 2010.

[25] E. R. Gelso and J. Lindberg, "Air-path model predictive control of a heavy-duty diesel engine with variable valve actuation", in *19th IFAC World Congress*, Cape Town, South Africa, Aug. 2014, pp. 3012–3017.

[26] E. R. Gelso and J. Dahl, "Diesel engine control with exhaust aftertreatment constraints", in *20th IFAC World Congress*, Toulouse, France, Jul. 2017, pp. 8921–8926.

[27] R. Cloudt and F. Willems, "Integrated emission management strategy for cost optimal engine-aftertreatment operation", *SAE International Journal of Engines*, vol. 4, pp. 1784–1797, 2011.

[28] F. Willems, P. Mentink, F. Kupper, and E. den Eijnden, "Integrated emission management for cost optimal EGR-SCR balancing in diesels", *IFAC Proceedings Volumes*, vol. 46, pp. 711–716, 2013.

[29]   M. Donkers, J. V. Schijndel, W. Heemels, and F. Willems, "Optimal control for integrated emission management in diesel engines", *Control Engineering Practice*, vol. 61, pp. 206–216, 2017.

[30]   E. Feru, N. Murgovski, B. de Jager, and F. Willems, "Supervisory control of a heavy-duty diesel engine with an electrified waste heat recovery system", *Control Engineering Practice*, vol. 54, pp. 190–201, Sep. 2016.

[31]   D. P. Bertsekas, *Dynamic Programming and Optimal Control*, Fourth. Athena Scientific, 2017.

[32]   EC. (Sep. 2016). Commission regulation (EU) 2016/1718, official journal of the european union L 259/1, [Online]. Available: `http://eur-lex.europa.eu/legal-content/EN/TXT/?uri=CELEX:32016R1718`.

[33]   R. M. Patil, J. C. Kelly, Z. Filipi, and H. K. Fathy, "A framework for the integrated optimization of charging and power management in plug-in hybrid electric vehicles", *IEEE Trans. Veh. Technol*, vol. 62, no. 6, pp. 2402–2412, Jul. 2013.

[34]   J. B. Rawlings, D. Q. Mayne, and M. M. Diehl, *Model Predictive Control: Theory, Computation, and Design*, 2nd ed. Nob Hill Publishing, LLC, 2019.

[35]   A. Hamednia, N. Murgovski, and J. Fredriksson, "Predictive velocity control in a hilly terrain over a long look-ahead horizon", *IFAC-PapersOnLine*, vol. 51, no. 31, pp. 485–492, 2018.

[36]   L. Johannesson, M. Nilsson, and N. Murgovski, "Look-ahead vehicle energy management with traffic predictions", *IFAC-PapersOnLine*, vol. 48, no. 15, pp. 244–251, 2015.

[37]   N. Murgovski, B. Egardt, and M. Nilsson, "Cooperative energy management of automated vehicles", *Control Engineering Practice*, vol. 57, pp. 84–98, 2016.

[38]   M. Hovgard, O. Jonsson, N. Murgovski, M. Sanfridson, and J. Fredriksson, "Cooperative energy management of electrified vehicles on hilly roads", *Control Engineering Practice*, vol. 73, pp. 66–78, 2018.

[39]   F. Zhang, X. Hu, R. Langari, and D. Cao, "Energy management strategies of connected hevs and phevs: Recent progress and outlook", *Progress in Energy and Combustion Science*, vol. 73, pp. 235–256, 2019.

[40]   A. Mayer, T. Lutz, C. Lämmle, M. Wyser, and F. Legerer, "Engine intake throttling for active regeneration of diesel particle", SAE International, Technical Paper 2003-01-0381, Mar. 2003.

[41]   P. Spurk *et al.*, "Examination of engine control parameters for the regeneration of catalytic activated diesel particulate filters in commercial vehicles", SAE International, Technical Paper 2003-01-3177, Oct. 2003.

[42]   A. Greszler. (Feb. 2008). Diesel turbo-compound technology, ICCT/NESCCAF Workshop on Improving the Fuel Economy of Heavy-Duty Fleets, [Online]. Available: `http://www.nescaum.org/documents/improving-the-fuel-economy-of-heavy-duty-fleets-1/`.

[43]   A. Boretti, "Dual fuel H2-diesel heavy duty truck engines with optimum speed power turbine", in *Proceedings of the FISITA 2012 World Automotive Congress*, Nov. 2012, pp. 77–99.

[44]   S. Gros, M. Zanon, R. Quirynen, A. Bemporad, and M. Diehl, "From linear to nonlinear mpc: Bridging the gap via the real-time iteration", *International Journal of Control*, vol. 93, no. 1, pp. 62–80, 2020.

Part II

Papers